Chapter 5
GAs and Nash GAs Using a Fast Meshless Method for CFD Design

Hong Wang, Hong-Quan Chen, and Jacques Periaux

Abstract Solving CFD inverse problems dealing with complex aerodynamic configurations like multi-element airfoils remains a difficult and expensive procedure, which requires seamless interfacing between several softwares like computer-aided design (CAD) system, mesh generator, flow analyzer, and an optimizer. It is essential to ensure the mesh quality during the optimization procedure for maintaining an accurate design. A fast meshless method using second and fourth order artificial dissipations and dynamic clouds of points based on the Delaunay graph mapping strategy is introduced to solve inverse computational fluid dynamics problems. The purpose of this paper is to use genetic algorithms and Nash genetic algorithms for position reconstructions of oscillating airfoils. The main feature of this paper is a detailed investigation on inverse problems in aerodynamics using both flexibility and efficiency of the fast meshless method. Comparisons of prescribed and computed aerodynamics parameters are presented for position reconstruction problems in aerodynamic design using both the fast meshless method coupled with artificial dissipation and a finite volume method. Numerical results are presented to illustrate the potential of the fast meshless method coupled with artificial dissipation and evo-

H. Wang (✉) · J. Periaux
Department of Mathematical Information Technology, University of Jyväskylä,
P.O. Box 35 (Agora), 40014 Jyväskylä, Finland
e-mail: hong.m.wang@jyu.fi

H.-Q. Chen
Department of Aerodynamics, Nanjing University of Aeronautics and Astronautics, 29 Yudao Jie,
Nanjing 210016, P.R. China
e-mail: hqchenam@nuaa.edu.cn

J. Periaux
International Center for Numerical Methods in Engineering (CIMNE), Edificio C1, Gran Captian,
s/n, 08034 Barcelona, Spain
e-mail: jperiaux@gmail.com

S. Repin et al. (eds.), *Numerical Methods for Differential Equations, Optimization, and Technological Problems*, Computational Methods in Applied Sciences 27,
DOI 10.1007/978-94-007-5288-7_5,

lutionary algorithms, to solve more complex optimization problems of industrial interest occurring in multidisciplinary design.

5.1 Introduction

Compared to direct computational fluid dynamics (CFD) problems, inverse problems [15] have been of ongoing interest to aerodynamic researchers. The position reconstruction is one of the important problems in high lift devices using multi element airfoils configurations. The goal of our present study is to implement efficiently on the computer a simple reconstruction problem with Genetic Algorithms (GAs) [10] and/or Nash GAs [11, 15] to reconstruct the target position of oscillating airfoils based on prescribed conditions.

Meshless methods (see, e.g., [2–9]) do not use the concept of mesh topology and provide more geometrical flexibility for computing flow fields. In addition, they are also useful in design optimization problems around complex configurations without constraints required by mesh quality and topology. A fast meshless method coupled with artificial dissipation (AD) using second and fourth order derivatives is employed for solving two-dimensional (2D) Euler equations. Spatial derivatives of the governing equations are approximated by a weighted least square (WLS) method discretizing the computational domain into clouds of points (see, e.g., [1–4]). An explicit five-stage Runge-Kutta scheme is utilized to reach the steady-state solution. A local time-stepping method and a residual averaging [3] are employed to accelerate the rate of convergence. Dynamic clouds of points based on the Delaunay graph mapping [8] are selected to ensure the flow field points following the movements of body boundaries.

The proposed approach is validated by comparing our numerical results against a finite volume method presented in [6] for a single oscillating NACA0012 airfoil. In this paper, we have tested the position reconstructions of oscillating airfoils operating in transonic regimes for aerodynamic design. Position reconstruction of a single airfoil has been tested using GAs optimizer. Position reconstruction of two airfoils has been tested with Nash GAs using both the fast meshless method coupled with AD and the finite volume method on the same computational nodes. Comparisons of prescribed and computed parameters are presented to show the efficacy of the fast meshless method coupled with AD and Nash game strategy in the position reconstruction problems in aerodynamic design.

The rest of the paper is organized as follows. Section 2 describes the methodology of the dynamic cloud method based on the Delaunay graph mapping strategy and the meshless method coupled with AD. Section 3 shows the validation of the proposed meshless method. Section 4 conducts two practical optimization applications and conclusions are presented in Sect. 5.

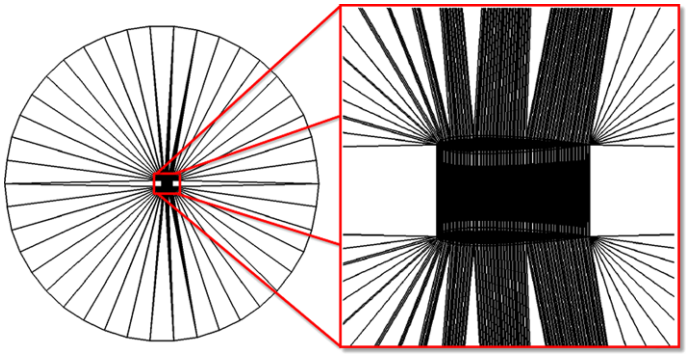

Fig. 5.1 Global and close-up views of a Delaunay graph in the case of NACA0012 airfoils

5.2 Methodology

5.2.1 Dynamic Cloud Method Based on the Delaunay Graph Mapping Strategy

In order to simulate the relative movement of boundaries in the position reconstruction, it is required that a cloud of points has the ability to move with the rigid body boundaries. Hence, a fast and efficient dynamic cloud method based on the Delaunay graph mapping strategy [8] is introduced here.

Firstly, as shown in Fig. 5.1, a Delaunay triangulation of the computational field is set up by using the given points located on the boundaries for BI-NACA0012 airfoils. Then, the triangulation is contained for every point $P(x, y)$ in the computational field. Notate the points of every element $E(x_1, y_1)$, $E(x_2, y_2)$ and $E(x_3, y_3)$, then the coordinates of the point can be expressed as

$$\begin{cases} x = a_1 x_1 + a_2 x_2 + a_3 x_3, \\ y = a_1 y_1 + a_2 y_2 + a_3 y_3, \end{cases} \tag{5.1}$$

where $a_1 = S_1/S$, $a_2 = S_2/S$, $a_3 = S_3/S$; S, S_1, S_2, S_3 are the relevant triangle's areas [8]. Then, all the background points by the movement of the boundary's points are adjusted. The coordinates of the relevant triangle become $E(x_1', y_1')$, $E(x_2', y_2')$ and $E(x_3', y_3')$, and the new coordinates of point can be denoted as

$$\begin{cases} x' = a_1 x_1' + a_2 x_2' + a_3 x_3', \\ y' = a_1 y_1' + a_2 y_2' + a_3 y_3'. \end{cases} \tag{5.2}$$

In [14] it is shown that better results can be obtained by using the Delaunay graph mapping strategy to ensure the flow field points following the movements of the body boundaries without any iteration. And compared to the spring analogy method described in [5].

5.2.2 Governing Equations

The so-called Euler equations represent the conservation principle for mass, momentum, and energy for inviscid fluids. In a 2D Cartesian coordinate system, Euler equations are expressed in the following form:

$$\frac{\partial \mathbf{W}}{\partial t} + \frac{\partial \mathbf{E}}{\partial x} + \frac{\partial \mathbf{F}}{\partial y} = 0, \tag{5.3}$$

where t denotes time and (x, y) the Cartesian coordinates. The expressions of conservative variables $\mathbf{W}$ and convective fluxes $\mathbf{E}$, $\mathbf{F}$ are introduced as

$$\mathbf{W} = \begin{bmatrix} \rho \\ \rho u \\ \rho v \\ e \end{bmatrix}, \qquad \mathbf{E} = \begin{bmatrix} \rho u \\ \rho u^2 + p \\ \rho uv \\ (e+p)u \end{bmatrix}, \qquad \mathbf{F} = \begin{bmatrix} \rho v \\ \rho uv \\ \rho v^2 + p \\ (e+p)v \end{bmatrix}, \tag{5.4}$$

where ρ denotes the density, u is the x-velocity component, v is the y-velocity component, p is the pressure, and e is the total energy per unit volume. For an ideal gas, e can be written as

$$e = \frac{p}{\gamma - 1} + \frac{1}{2}\rho\left(u^2 + v^2\right),$$

where γ is the ratio of specific heat. Additionally, the equation of state is given by

$$p = \rho \bar{R} T,$$

where T is the static temperature and $\bar{R}$ is the ideal gas constant.

5.2.3 Spatial Discretization

The WLS method [4] is used to approximate the spatial first-order derivatives, and in the cloud $C(i)$ as shown in Fig. 5.2, (5.3) becomes

$$\left.\frac{\partial \mathbf{W}}{\partial t}\right|_i + \left(\frac{\partial \mathbf{E}}{\partial x} + \frac{\partial \mathbf{F}}{\partial y}\right)_i = 0. \tag{5.5}$$

For the convective fluxes, let

$$\mathbf{Q}_i = \left(\frac{\partial \mathbf{E}}{\partial x} + \frac{\partial \mathbf{F}}{\partial y}\right)_i. \tag{5.6}$$

According to the WLS method [4], (5.6) could be written as

$$\mathbf{Q}_i = \sum \alpha_{ik} \mathbf{E}_{ik} + \sum \beta_{ik} \mathbf{F}_{ik}. \tag{5.7}$$

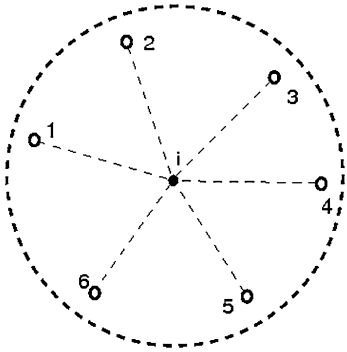

Fig. 5.2 A typical structure of the cloud $C(i)$

Then the governing equation can be written as

$$\frac{d\mathbf{W}_i}{dt} = -\left(\mathbf{Q}_i - \sum_{k=1}^{N} d_{ik}\right), \tag{5.8}$$

where [3]

$$\begin{aligned}
d_{ik} &= \epsilon_{ik}^{(2)}(\mathbf{W}_k - \mathbf{W}_i) - \epsilon_{ik}^{(4)}\left(\nabla^2\mathbf{W}_k - \nabla^2\mathbf{W}_i\right),\\
\epsilon_{ik}^{(2)} &= K^{(2)}\lambda_{ik}\max(\upsilon_i, \upsilon_k),\\
\epsilon_{ik}^{(4)} &= \lambda_{ik}\max\left[0, K^{(4)} - \epsilon_{ik}^{(2)}\right],\\
\upsilon_i &= \frac{|\nabla^2 P_i|}{\sum_{k=1}^{N}(P_i + P_k)},\\
\nabla^2\mathbf{W}_i &= \sum_{k=1}^{N}\mathbf{W}_k - N\mathbf{W}_i,\\
\lambda_{ik} &= |\alpha_{ik}u + \beta_{ik}v| + c\sqrt{\alpha_{ik}^2 + \beta_{ik}^2}.
\end{aligned}$$

Here $c = \sqrt{\gamma p/\rho}$ is the local speed of sound.

5.2.4 Temporal Discretization

Within the cloud $C(i)$, the semi-discretisation Euler equations are rewritten as

$$\left.\frac{\partial \mathbf{W}}{\partial t}\right|_i = \mathbf{R}_i, \tag{5.9}$$

where $\mathbf{R}_i$ means the residual value. An explicit scheme is used for time discretisation in (5.9), and we get

$$\frac{\mathbf{W}_i^{n+1} - \mathbf{W}_i^n}{\Delta t} = \mathbf{R}_i. \tag{5.10}$$

The superscripts n and $(n+1)$ denote the time levels. Hence, $\mathbf{W}^n$ means the flow solution at the present time t, and $\mathbf{W}^{n+1}$ represents the solution at the time $(t + \Delta t)$. An explicit five-stage Runge-Kutta time integration scheme is used

$$\begin{cases} \mathbf{W}_i^{(0)} = \mathbf{W}_i^n, \\ \mathbf{W}_i^{(1)} = \mathbf{W}_i^{(0)} + \alpha_1 \Delta t_i \mathbf{R}_i^{(0)}, \\ \mathbf{W}_i^{(2)} = \mathbf{W}_i^{(0)} + \alpha_2 \Delta t_i \mathbf{R}_i^{(1)}, \\ \mathbf{W}_i^{(3)} = \mathbf{W}_i^{(0)} + \alpha_3 \Delta t_i \mathbf{R}_i^{(2)}, \\ \mathbf{W}_i^{(4)} = \mathbf{W}_i^{(0)} + \alpha_4 \Delta t_i \mathbf{R}_i^{(3)}, \\ \mathbf{W}_i^{(5)} = \mathbf{W}_i^{(0)} + \alpha_5 \Delta t_i \mathbf{R}_i^{(4)}, \\ \mathbf{W}_i^{n+1} = \mathbf{W}_i^{(5)}, \end{cases} \tag{5.11}$$

where α_k, $k = 1, 2, 3, 4, 5$, represents the stage coefficients, and we have $\alpha_1 = \frac{1}{4}$, $\alpha_2 = \frac{1}{6}$, $\alpha_3 = \frac{3}{8}$, $\alpha_4 = \frac{1}{2}$, $\alpha_5 = 1$.

The major disadvantage of the explicit scheme is that the time step is restricted by the Courant-Friedrichs-Lewy (CFL) stability condition [3].

5.2.5 Acceleration Techniques

In order to accelerate the convergence, a local time stepping method and an implicit residual averaging method are employed in our present work. The local time step Δt_i of a discrete point is given by the equation [3, 12, 13]

$$\Delta t = \frac{C_{\mathrm{CFL}}}{\sum_{k=1}^{N} |\alpha_{ik} u + \beta_{ik} v| + c\sqrt{\alpha_{ik}^2 + \beta_{ik}^2}}, \tag{5.12}$$

where C_{CFL} denotes the coefficient of CFL.

In the meshless method for the time marching equation, let $\mathbf{R}_i$ represent the residual at node i. The new residual [3] can be given as

$$\mathbf{R}_i' = \frac{\mathbf{R}_i + \epsilon \sum_{k=1}^{M} \mathbf{R}_k'}{1 + \epsilon M}, \tag{5.13}$$

where $\epsilon = [0.2, 0.5]$ and it can be obtained by performing two Jacobi iterations. The above technique allows the CFL number to be increased twofold or threefold when

compared to the unsmoothed value, and consequently the CFL number is increased from $2\sqrt{2}$ to 5 in the present study.

5.3 Validation of the Fast Meshless Method Implemented with Artificial Dissipation (AD)

In order to validate the proposed fast meshless method coupled with AD, a single NACA0012 airfoil operating with flow conditions at a 3.0° angle of attack and a Mach number 0.5 is tested. Figure 5.3 provides both the global view and the close-up view of the cloud of points distributed around one single NACA0012 airfoil, and Fig. 5.4 shows both the global view and the close-up view of the mesh distributed for the same airfoil. There are 5047 nodes in the whole computational domain in the meshless method and 9762 elements in the mesh method. Figure 5.5 shows the comparison of surface pressure coefficients for this test case using the fast meshless method coupled with AD and the finite volume method in [6].

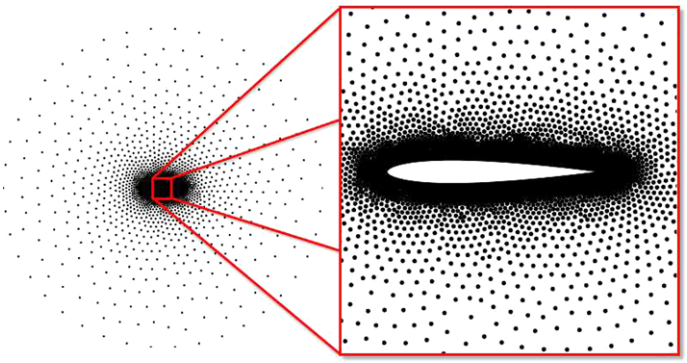

Fig. 5.3 Global and close-up views of the cloud of points for the NACA0012 airfoil

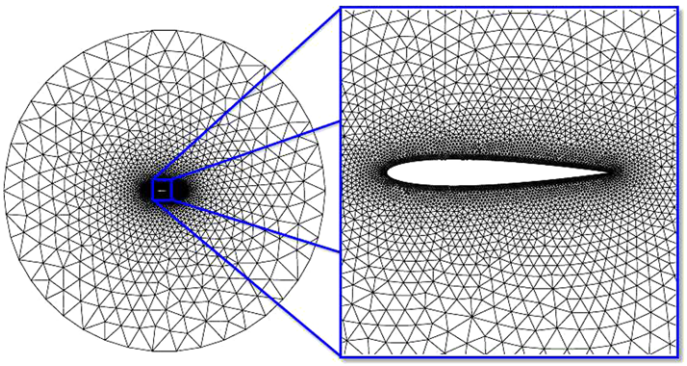

Fig. 5.4 Global and close-up views of the mesh for the NACA0012 airfoil

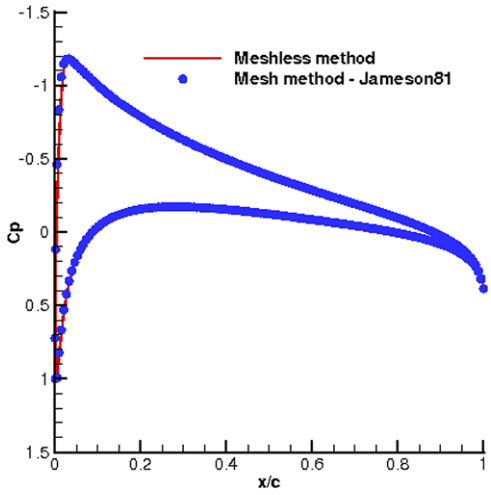

Fig. 5.5 Comparisons of surface pressure coefficients for the NACA0012 airfoil

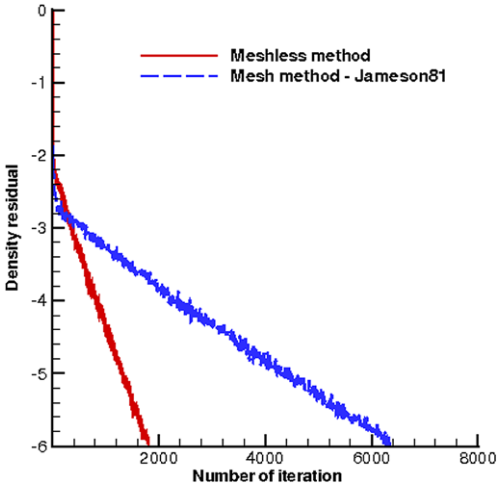

Fig. 5.6 Comparisons of the convergence history for the NACA0012 airfoil

Figure 5.6 shows the comparison of the convergence history for this case using the fast meshless method coupled with AD and the referenced mesh method [6]. As shown in the histogram in Figs. 5.7 and 5.8, the meshless method coupled with AD in this test case saves 71.5 % in the iteration costs compared to the finite volume method described in [6]. In terms of the CPU time needed in this test case, the meshless method coupled with AD saves 65.7 % compared to the finite volume method in [6]. The computer hardware used in this paper is an Intel(R) Core(TM) with 2 Quad CPU Q9650 with frequency 2.00 GHz/2.99 GHz and 3.00 GB of RAM.

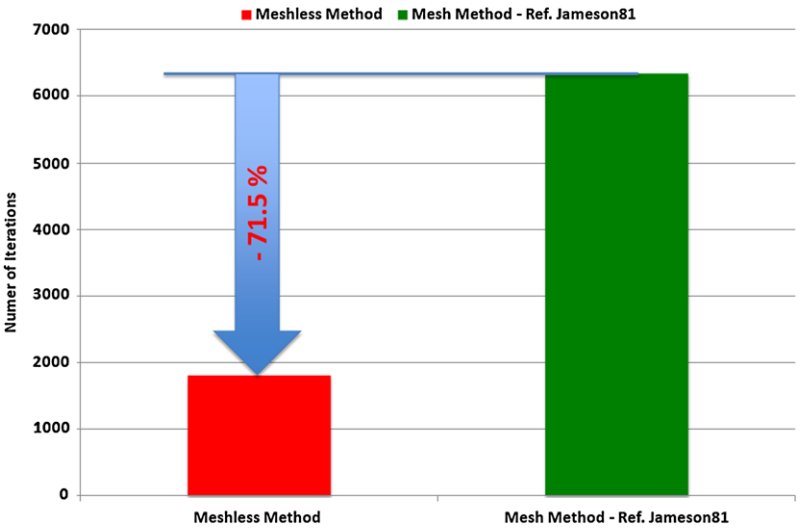

Fig. 5.7 Comparisons of the convergence history in terms of the number of iterations for the NACA0012 airfoil

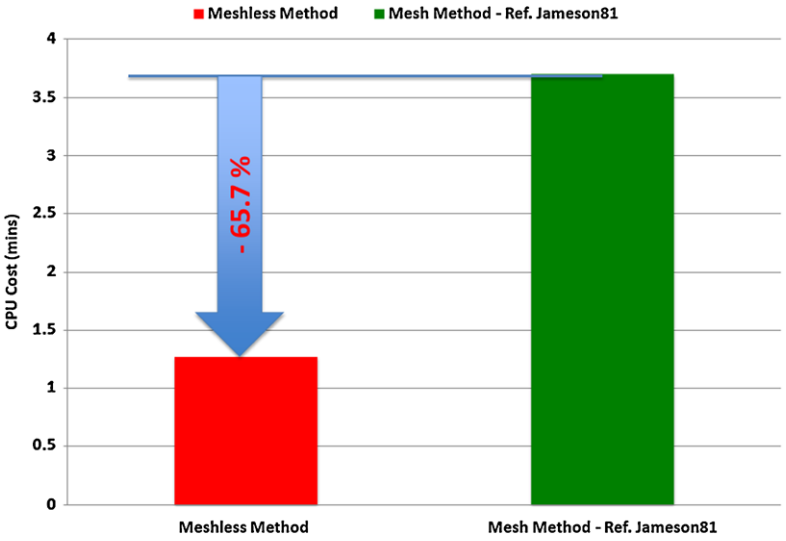

Fig. 5.8 Comparisons of the convergence history in terms of the CPU cost for the NACA0012 airfoil

5.4 Practical Optimization Applications

In this section, both the fast meshless method coupled with AD and the finite volume method referenced in [6] are used to test two inverse position reconstruction problems: a single pitching NACA0012 airfoil and BI-NACA0012 airfoils.

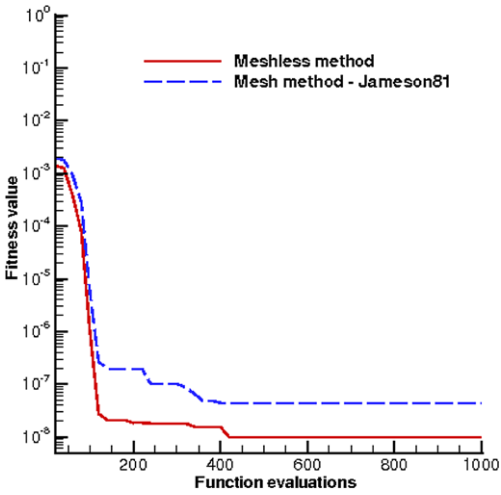

Fig. 5.9 Comparisons of the convergence history in terms of fitness value for a single NACA0012 airfoil

5.4.1 A Single Pitching NACA0012 Airfoil

Let one airfoil oscillate in pitch about its quarter chord, and the rotating angle α is selected as the design parameter. The objective function is defined according to the surface pressure coefficients as

$$\min f(\alpha) = \sum_{i=1}^{M} \left| C_p(\alpha) - C_p\left(\alpha^*\right) \right|_i^2, \tag{5.14}$$

where M is the total number of points distributed on the surface of an airfoil, the search space is $\alpha \in [-10.0°, 10.0°]$, and α^* is the prescribed design variable. Parameters of the GAs optimizer are chosen as: the size of population is 20, the probability of crossover is 0.85, and the probability of mutation is 0.01.

The flow conditions of the reconstruction test case are as follows: the Mach number is 0.8 and the target angle of attack is 0.0°. Figure 5.9 shows the convergence history of fitness value during the reconstruction process using the fast meshless method coupled with AD and the finite volume method in [6] separately. As shown on the histogram of Fig. 5.10, the meshless method coupled with AD saves 69.7 % compared to the finite volume method referenced in [6] in terms of the CPU time cost.

5.4.2 BI-NACA0012 Airfoil's Configuration

Let two airfoils oscillate in pitch about their quarter chords, and rotating angles α_1, α_2 are selected as design parameters. The two objective functions defined in a

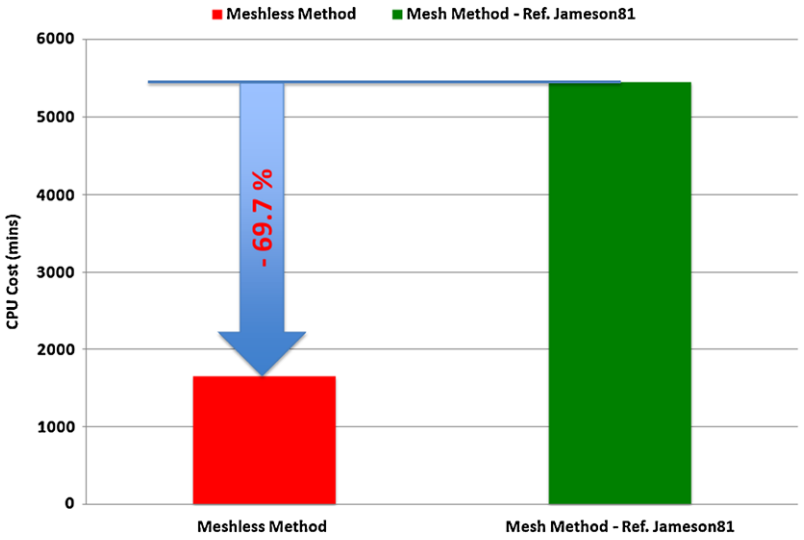

Fig. 5.10 Comparisons of the convergence history in terms of the CPU cost for the NACA0012 airfoil

reconstruction problem solved by the Nash-GAs optimizer are

$$\min f_1(\alpha_1, \alpha_2^{**}) = \sum_{i=1}^{M_1} \left| C_p(\alpha_1) - C_p(\alpha_1^*) \right|_i^2 + \sum_{i=1}^{M_2} \left| C_p(\alpha_2^{**}) - C_p(\alpha_2^*) \right|_i^2, \quad (5.15)$$

$$\min f_2(\alpha_1^{**}, \alpha_2) = \sum_{i=1}^{M_1} \left| C_p(\alpha_1^{**}) - C_p(\alpha_1^*) \right|_i^2 + \sum_{i=1}^{M_2} \left| C_p(\alpha_2) - C_p(\alpha_2^*) \right|_i^2, \quad (5.16)$$

where M_1 is the total number of points distributed on the surface of the upper airfoil while M_2 is the total number of points distributed on the surface of the lower airfoil, the search spaces are $\alpha_1 \in [-10.0°, 10.0°]$, $\alpha_2 \in [-10.0°, 10.0°]$, and α_1^*, α_2^* are prescribed parameters. The parameters in Nash GAs are chosen as follows: the size of the population is 10, the probability of crossover is 0.85, and the probability of mutation is 0.02.

The Euler flow conditions around the BINACA0012 configuration are the following: the Mach number is 0.5 and the prescribed parameters are 0.0° and 0.0°. Figure 5.11 shows the convergence history of the objective function during the reconstruction process using Nash GAs based on the meshless method coupled with AD and the finite volume method in [6]. As shown in the histogram in Fig. 5.12, the meshless method coupled with AD saves 75.8 % compared to the finite volume method in [6] in terms of the CPU time cost.

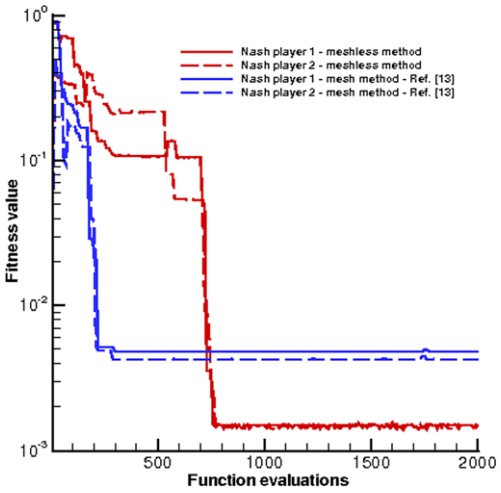

Fig. 5.11 Comparisons of the convergence history for BINACA0012 airfoils in terms of the objective function using the fast meshless method coupled with AD and the standard mesh method

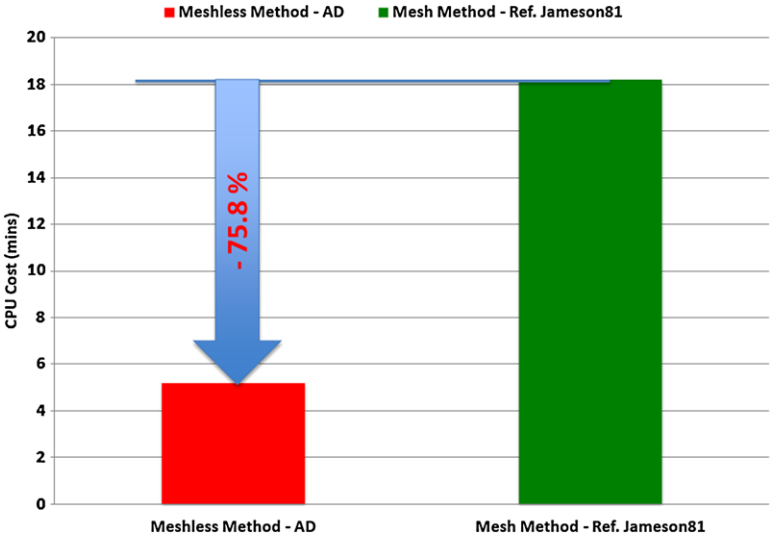

Fig. 5.12 Comparisons of the convergence history in terms of the CPU cost for the BI-NACA0012 airfoils

5.5 Conclusions and Future

A fast Euler meshless method using artificial dissipations is used in this paper. Dynamic clouds of points based on a Delaunay graph mapping strategy have been introduced to ensure that flow field points can easily follow the movements of solid body boundaries. Position reconstructions of oscillating airfoils operating in transonic regimes have been tested for future aerodynamic design like high lift devices. First a single airfoil position reconstruction has been tested successfully with a sim-

ple GAs optimizer. Then, position reconstruction of two airfoils has been tested with Nash GAs using both the fast meshless method coupled with AD and the finite volume method referenced in [6] using the same number of computational nodes. Comparisons of target geometries and computed parameters are presented to prove the superiority of the meshless Euler flow analyzer methods implemented with AD coupled with the Nash evolutionary optimizer for position reconstruction inverse problems in aerodynamic design. This study is a roadmap to more complex design optimization problems which can benefit of game coalitions [7] in terms of accuracy and efficiency.

References

1. Batina JT (1992) A fast implicit upwind solution algorithm for three-dimensional unstructured dynamics meshes. AIAA paper 1992-447
2. Batina JT (1993) A gridless Euler/Navier-Stokes solution algorithm for complex-aircraft applications. AIAA paper 1993-333
3. Blazek J (2001) Computational fluid dynamics: principles and applications. Elsevier, Amsterdam
4. Chen HQ (2003) Implicit gridless method for Euler equations. Chin J Comput Phys 20(1):9–13
5. Farhat C, Degand C, Koobus B, Lesoinne M (1998) An improved method of spring analogy for dynamic unstructured fluid meshes. AIAA paper 1998-2070
6. Jameson A, Schmidt W, Turkel E (1981) Numerical solution of the Euler equations by finite volume methods using Runge-Kutta time-stepping schemes. In: AIAA 14th fluid and plasma dynamics conference, Palo Alto, CA, 1981
7. Lee DS, Gonzalez LF, Periaux J, Srinivas K (2011) Efficient hybrid-game strategies coupled to evolutionary algorithms for robust multidisciplinary design optimization in aerospace engineering. IEEE Trans Evol Comput 15(2):133–150
8. Liu XQ, Qin N, Xia H (2006) Fast dynamic grid deformation based on Delaunay graph mapping. Chin J Comput Phys 211(2):405–423
9. Ma ZH, Chen HQ, Wu XJ (2006) A gridless-finite volume hybrid algorithm for Euler equations. Chin J Aeronaut 19(4):286–294
10. Michalewicz Z (1992) Genetic algorithms + data structures = evolution programs. Springer, Berlin
11. Nash J (1951) Non-cooperative games. Ann Math 54:286–295
12. Pulliam TH (1986) Artificial dissipation models for the Euler equations. AIAA J 24(12):1931–1940
13. Pulliam TH, Steger JL (1985) Recent improvements in efficiency, accuracy, and convergence for implicit approximate factorization algorithms. AIAA paper 1985-360
14. Wang H, Chen HQ, Periaux J (2010) A study of gridless method with dynamic clouds of points for solving unsteady CFD problems in aerodynamics. Int J Numer Methods Fluids 64(1):98–118
15. Wang JF, Wu YZ, Periaux J (2002) Genetic algorithms and game theory for high lift design problems in aerodynamics. Trans Nanjing Univ Aeronaut Astronaut 19(1):7–13